

Testing general relativity using binary extreme-mass-ratio inspirals

Wen-Biao Han,^{1,2} and Xian Chen^{3,4}★

¹Shanghai Astronomical Observatory, Shanghai 200030, China

²School of Astronomy and Space Science, University of Chinese Academy of Sciences, Beijing 100049, China

³Astronomy Department, School of Physics, Peking University, Beijing 100871, China

⁴Kavli Institute for Astronomy and Astrophysics at Peking University, Beijing 100871, China

Accepted XXX. Received YYY; in original form ZZZ

ABSTRACT

It is known that massive black holes (MBHs) of $10^{5-7} M_{\odot}$ could capture small compact objects to form extreme-mass-ratio inspirals (EMRIs). Such systems emit gravitational waves (GWs) in the band of the Laser Interferometer Space Antenna (LISA) and are ideal probes of the space-time geometry of MBHs. Recently, we have shown that MBHs could also capture stellar-mass binary black holes (about $10 M_{\odot}$) to form binary-EMRIs (b-EMRIs) and, interestingly, a large fraction of the binaries coalesce due to the tidal perturbation by the MBHs. Here we further show that the coalescence could be detected by LISA as glitches in EMRI signals. We propose an experiment to use the multi-band (10^2 and 10^{-3} Hz) glitch signals to test gravity theories. Our simulations suggest that the experiment could measure the mass and linear momentum lost via GW radiation, as well as constrain the mass of gravitons, to a precision that is one order of magnitude better than the current limit.

Key words: black hole physics – gravitational waves – methods: analytical – stars: kinematics and dynamics

1 INTRODUCTION

Extreme-mass-ratio inspirals (EMRIs) are important gravitational-wave (GW) sources in the milli-Hertz band (Amaro-Seoane et al. 2007; Babak et al. 2017). It is produced when a massive black hole (MBH) captures a small compact object, normally a stellar-mass black hole (BH) of $\sim 10 M_{\odot}$, to a tightly bound orbit (Amaro-Seoane et al. 2007). Because of gravitational radiation, the small body spirals in towards the MBH until the last stable orbit, from which point on it plunges into the central hole. The GW signal produced in the final $10^4 - 10^5$ orbital cycles encodes rich information about the space-time geometry at the immediate exterior of the MBH (Gair et al. 2013; Barausse et al. 2014) and is detectable by a space-borne GW detector, such as the Laser Interferometer Space Antenna (LISA).

Recent studies indicate that in as many as 10% of EMRIs the captured small bodies in fact could be stellar-mass binary BHs (BBHs) (Addison et al. 2015; Chen & Han 2018). These binaries initially form far away from the MBHs but later are scattered by other stars to the vicinity of the MBHs and become captured due to tidal interactions. Numerical simulations showed that about 30% of

the BBHs would coalesce at a close distance to the MBHs due to the tidal perturbation (Chen & Han 2018). Interestingly, the coalescence would produce high-frequency (10^2 Hz) GW signals, i.e., LIGO/Virgo events, which would occur at the same time, sky location and luminosity distance as the low-frequency (10^{-3} Hz) EMRIs. These binary-EMRIs (b-EMRIs) are new targets for future multi-band GW observations (Sesana 2016).

According to general relativity, if BBHs coalesce the post-merger BHs will recoil because GWs carry linear momentum and the GW radiation from BBHs is normally asymmetric (Fitchett 1983). The magnitude of the recoil velocity is a function of the mass ratio of the two merging BHs as well as their spin magnitudes and directions (see fitting formulae in Favata et al. 2004; Blanchet et al. 2005; Baker et al. 2006; Sopuerta et al. 2006; Damour & Gopakumar 2006; Koppitz et al. 2007; González et al. 2007a,a,b; Campanelli et al. 2007; Schnittman & Buonanno 2007; Baker et al. 2008; Rezzolla et al. 2008; Schnittman et al. 2008; van Meter et al. 2010; Lousto & Zlochower 2011, and a review in Centrella et al. 2010). For a mass ratio close to unity, which the current LIGO/Virgo observations seem to prefer (The LIGO Scientific Collaboration & the Virgo Collaboration 2018), the recoil velocity lies in a broad range of $v \in (200, 10^3) \text{ km s}^{-1}$ with a mean value of about 400 km s^{-1} ,

★ E-mail: xian.chen@pku.edu.cn

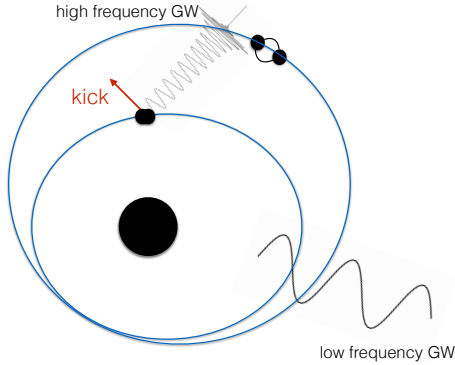


Figure 1. Physical picture of a glitch in a b-EMRI. The black-hole binary, initially moving on an eccentric orbit, circularizes around the MBH due to GW radiation and later coalesces due to the tidal perturbation by the MBH. The motion of the binary around the MBH generates low-frequency ($\sim 10^{-3}$ Hz) GWs and the coalescence of the two small BHs produces high-frequency ($\sim 10^2$ Hz) waves. The coalescence also induces a kick to the velocity of the remnant black hole. As a result, a glitch appears in the low-frequency waveform.

according to our earlier calculations using random orientation and magnitude for the spin parameters (Amaro-Seoane & Chen 2016).

In this paper, we show that such a recoil velocity will significantly alter the orbital elements of the small bodies in b-EMRIs so that glitches are induced in the low-frequency EMRI waveforms. We simulate LISA observation of the b-EMRIs and find that the glitches can be detected within half a day. Moreover, we propose to use the glitch signals to (1) measure the corresponding recoil velocity to a precision of 10 km s^{-1} , (2) constrain the amount of rest mass that is lost via GW radiation to an accuracy of 1.5% and (3) improve the current constraint by LIGO/Virgo on the graviton mass by one order of magnitude. Throughout the paper we adopt the convention $G = c = 1$.

2 PHYSICAL PICTURE

The system of our interest is described in Chen & Han (2018) and the physical picture is illustrated in Figure 1. The BBH initially is moving on an eccentric orbit close to the central MBH and later coalesces due to the tidal perturbation. The coalescence generates high-frequency GWs and causes the remnant BH to recoil.

Figure 2 suggests that when the small body recoils, the low-frequency GWs associated with its orbit around the MBH are detectable by LISA. This result is derived from the facts that (1) the GW radiation comes mostly from the orbital pericentre (Wen 2003) and (2) the pericentres of the small bodies in b-EMRIs are typically $10 - 10^3$ gravitational radii of the central MBHs, corresponding to an orbital frequency of about $10^{-4} - 10^{-2}$ Hz.

The recoil affects the orbital eccentricity of the small body around the MBH and hence disturbs the low-frequency

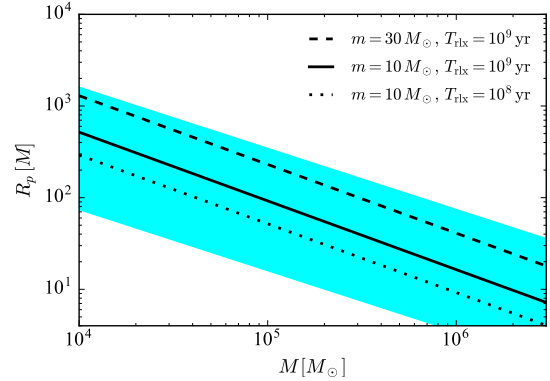


Figure 2. Pericenter distances (R_p) of the small bodies in b-EMRIs as a function of the mass M of the MBHs. The distances are in unit of the gravitational radii of the central MBHs and are computed according to our earlier model of the dynamical formation of b-EMRIs (Chen & Han 2018). The dashed, solid and dotted lines refer to models with different mass, m , for the stellar black holes and different relaxation timescale, T_{tik} , for the star cluster surrounding the MBH. For simplicity, we consider only equal-mass binaries. The cyan shaded area corresponds to the sensitive band of a LISA-type detector, which covers $10^{-4} - 10^{-2}$ Hz. The upper and lower boundaries of the sensitive band are computed using Equation (37) in Wen (2003), which relates the frequency of the strongest GW harmonic to R_p and e .

GW signal. It is known that LISA can measure the eccentricities of EMRIs to a precision of about $\Delta e \sim 10^{-6} - 10^{-4}$ (Babak et al. 2017). In our case, if the recoil velocity is in the polar or azimuthal direction (corresponding to v_θ or v_ϕ in the Boyer-Lindquist coordinate), the eccentricity changes by an amount of

$$\Delta e \approx \frac{v}{\sqrt{M/R}} \sqrt{\frac{1-e^2}{e}} \approx 4.2 \times 10^{-3} \sqrt{\frac{1-e^2}{e}} \times \left(\frac{v}{400 \text{ km s}^{-1}} \right) \left(\frac{R}{10 M} \right)^{1/2} \quad (1)$$

where R is the distance between the small remnant BH and the MBH when the recoil happens. If the recoil velocity is in the radial direction (v_r), we find

$$\Delta e \approx \frac{Rv^2}{M} \left(\frac{1-e^2}{2e} \right) \approx 8.9 \times 10^{-6} \left(\frac{1-e^2}{e} \right) \times \left(\frac{v}{400 \text{ km s}^{-1}} \right)^2 \left(\frac{R}{10 M} \right). \quad (2)$$

The above order-of-magnitude estimations suggest that the recoil can indeed produce a glitch in the low-frequency waveform that is detectable by LISA.

3 RESOLVING THE GLITCH

To simulate the glitch signals from b-EMRIs, we first notice that the glitches happen almost instantaneously: They are produced during the last second of BBH mergers, while the EMRI waveforms normally last months to years. For this reason, we construct the glitched waveforms in the following two steps. First, we compute the waveform of a standard

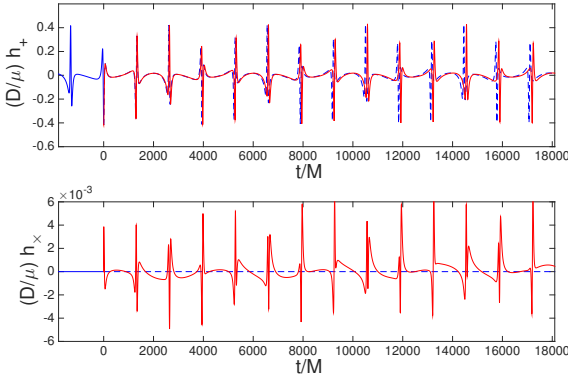


Figure 3. Comparing the waveforms of the EMRIs with (red) and without (blue) a glitch. The upper and lower panels are showing the two polarizations. The MBH has a mass of $M = 10^6 M_\odot$ and a spin parameter of 0.9. The total mass of the stellar-black-hole binary is $m = 20 M_\odot$, and D refers to the luminosity distance. In this example, the centre-of-mass of the stellar-mass BBH initially is moving inside the equatorial plane of the MBH with an orbital eccentricity of $e = 0.7$ and a semi-latus rectum of $p \equiv R(1 - e^2) = 17 M$. At the time $t = 0$ we introduce a kick to the centre-of-mass velocity of the binary, in the polar direction and with a magnitude of 1500 km s^{-1} . As a result, the orbital parameters changes to $p = 16.9990M$ and $e = 0.7019$, and the orbital plane of the EMRI becomes inclined by $\iota = 0.5233^\circ$ relative to the equatorial plane of the MBH. This inclination gives rise to the “x” polarization.

EMRI using an augmented analytical kludge (AAK) model (Chua et al. 2017) and evolve it for a few months. In the calculation we assume that the stellar-mass BBH can be approximated by a single body with a mass equal to the total mass of the BBH. This approximation is valid because months before the merger the BBH is already so compact that the tidal force exerted by the MBH on the binary is dynamically unimportant for the subsequent evolution of the triple system (Chen et al. 2017). Second, we introduce a perturbation to the orbital elements of the EMRI, to mimic the effects of the recoil, and then continue integrating the system with the new parameters. In this section we do not consider mass loss during the merger, i.e., the mass of the BH after the merger is assumed to be the same as the total BH mass before the merger. We will consider the effect of mass loss in the next section.

Figure 3 shows one example of the glitched waveform where an extreme recoil velocity of $v_\theta = 1500 \text{ km s}^{-1}$ is introduced at the $t = 0$. We see that within a time of $1.8 \times 10^4 M$ the glitch is visible to the naked eye. This duration corresponds to only 25 hours for a system with a MBH of $10^6 M_\odot$. The missing of the “x” polarization in the initial condition is caused by our choice of the line-of-sight, which is aligned with the orbital plane of the EMRI (edge-on view). The “x” polarization arises after the merger because the polar recoil tilts the orbital plane by a small angle.

For recoil velocities much smaller than 1500 km s^{-1} , the difference between the glitched and non-glitched waveforms is less prominent. More sophisticated methods are needed to detect the mismatch. LISA uses a technique called the “matched filtering” to search for any deviation between a signal $a(t)$ and a model waveform $b(t)$ (Finn 1992; Hughes

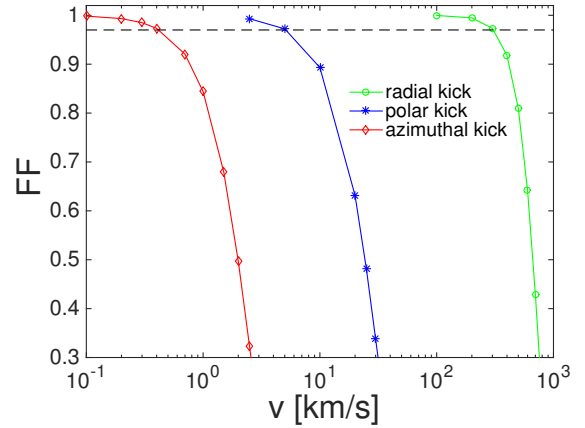


Figure 4. Fitting factor (FF) as a function of the recoil velocity. Different curves refer to kicks in different directions. The horizontal dashed line corresponds to a FF of 0.97. The mass and spin parameters of the BHs are the same as in Figure 3. The orbital parameters before the recoil is $p = 17.1395M$, $e = 0.6970$ and $\iota = 4.8968^\circ$.

2000; Drasco & Hughes 2006; Sundararajan et al. 2007; Glampedakis & Kennefick 2002; Fujita et al. 2009; Han 2010; Han & Cao 2011; Han 2014; Cao & Han 2017; Han et al. 2017; Barack & Cutler 2004; Gair & Glampedakis 2006; Babak et al. 2007). In our problem, $a(t)$ is the waveform containing a glitch and $b(t)$ is the one without a glitch. We generate them using the polarizations $h(t) = h_+(t) - ih_\times(t)$. The similarity of the two waveforms can be quantified by the fitting factor (FF),

$$\text{FF} = \frac{(a|b)}{\sqrt{(a|a)(b|b)}}, \quad (3)$$

where the inner product $(a|b)$ is computed with

$$(a|b) = 4 \int_0^\infty \frac{\tilde{a}(f)\tilde{b}^*(f)}{S_n(f)} df. \quad (4)$$

The tilde symbols in the last equation stand for the Fourier transform and the star for the complex conjugation. The quantity $S_n(f)$ is the spectral noise density for LISA (from Larson et al. 2000). An exact match corresponds to a FF of 1 and a complete mismatch leads to $\text{FF} = 0$. A good match normally requires $\text{FF} > 0.97$.

Figure 4 shows the FF as a function of the magnitude and direction of the recoil velocity \mathbf{v} . The lengths of the waveforms are five days, starting from the merger of the binary BHs, and the sampling frequency is 0.4 Hz. We find that the FF becomes worse when the recoil velocity increases. Moreover, azimuthal kicks cause the biggest mismatch. Using $\text{FF} < 0.97$ as a criterion for mismatch, we find that the minimum detectable velocity is about 0.4, 4, and 300 km s^{-1} , respectively, when the recoil is in the azimuthal, polar, and radial direction. In a realistic situation, the recoil velocity has a random direction and a typical magnitude of \mathbf{v} is $\mathcal{O}(10^2) \text{ km s}^{-1}$ (Amaro-Seoane & Chen 2016). Therefore, we expect the FF to diminish and the original EMRI signal completely lost after the glitch.

To see how accurately we can pinpoint the time of the

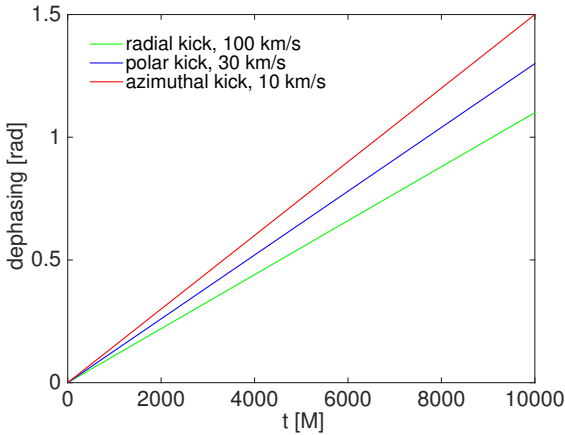


Figure 5. Dephasing between the waveforms with and without a glitch. The recoil is introduced at the time $t = 0$. The initial conditions are the same as in Figure 4.

recoil, we compare the waveforms with and without a glitch and evaluate the degree of mismatch (known as “dephasing”) as a function of time. The results are shown in Figure 5. We find that the mismatch grows the fastest for azimuthal kicks. LISA can discern a mismatch as small as one radian if the EMRI stays in the LISA band for about one year (Gair et al. 2013). Such an accuracy corresponds to a time resolution of (6000 – 9000) M according to Figure 5, or 8 – 13 hours in a system with a MBH of $M = 10^6 M_\odot$.

We note that although the original EMRI is lost due to the mismatch, a new one—from the same sky location, luminosity distance and with almost the same BH masses—will emerge immediately after the glitch because the recoiling BH remains bound to the MBH. This second EMRI can be detected by LISA with a signal-to-noise ratio (SNR) comparable to the old one since the GW amplitudes before and after the glitch are of the same order of magnitude (e.g., the top panel of Figure 3). Finding the second EMRI can rule out many other possibilities for the physical cause of the glitch, such as instrumental glitch or plunge of the small body into the MBH. One contamination could be a glitch in a standard EMRI which is induced by a stellar interloper (Amaro-Seoane et al. 2012), but such a glitch does not have a LIGO/Virgo counterpart (see next section).

4 TESTING GENERAL RELATIVITY

By modeling a glitched waveform, we can derive not only the time when the glitch happens, but also the recoil velocity (v) and the amount of rest mass (Δm) that is lost during the merger of the two stellar BHs (because GWs also carry away energy (Tichy & Marronetti 2008)). Figure 6 shows an example of measuring v and Δm using a glitched b-EMRI waveform. In this simulation, a recoil velocity of $v_\phi = 10 \text{ km s}^{-1}$ is introduced at $t = 0$. Moreover, we assume that each stellar BH has a mass of $10 M_\odot$ and during the merger a rest mass of $\Delta m = 1 M_\odot$ is lost. The other initial conditions are the same as in Figure 3. We compute the waveform of a duration of six months with a SNR of 30, which corresponds to a distance of 50 Mpc to the b-EMRI. Given such a large SNR,

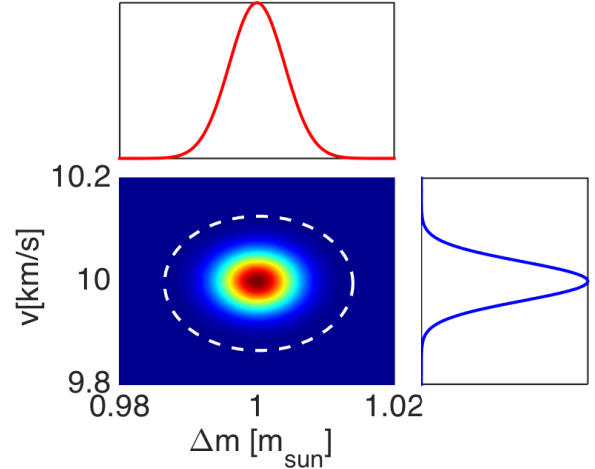


Figure 6. Likelihood of the recoil velocity v and mass loss Δm derived from the Fisher matrix. The white dashed ellipse shows the $3 - \sigma$ confidence level. The upper and right panels show the marginalized probability distribution for Δm and v , respectively.

the errors for parameter estimation can be approximated by the square root of the diagonal elements of the inverse of the Fisher matrix Γ_{ij} , where

$$\Gamma_{ij} = \left(\frac{\partial h}{\partial \lambda_i} \middle| \frac{\partial h}{\partial \lambda_j} \right) \quad (5)$$

(see Cutler & Flanagan 1994, for details), and $\lambda_1 = \Delta m$ and $\lambda_2 = v$. The corresponding likelihood is

$$\mathcal{L}(\lambda) \propto e^{-\frac{1}{2} \Gamma_{ij} \Delta \lambda_i \Delta \lambda_j}. \quad (6)$$

(e.g. Cutler & Flanagan 1994; Babak et al. 2017).

The plot of the likelihood suggests that we can detect a recoil velocity as small as 10 km s^{-1} and measure the mass loss to an accuracy of about 1.5%. For comparison, earlier works propose to use the GWs from isolated binaries (without MBHs) to measure v and Δm . The minimum recoil velocity those methods can detect is $\Delta v \simeq (120 - 200) \text{ km s}^{-1}$ (Gerosa & Moore 2016; Calderón Bustillo et al. 2018) and the accuracy in measuring the mass loss is typically (10 – 30)% (Abbott et al. 2016; The LIGO Scientific Collaboration & the Virgo Collaboration 2018). Therefore, using b-EMRIs we can improve the test of v and Δm by one order of magnitude.

Detecting b-EMRIs also enable us to test gravity theories alternative to classic GR. For example, in GR, GWs travel at the speed of light. In quantum gravity, however, the speed depends on the mass of gravitons, which is a function of the frequency of GWs (Will 1998). Since b-EMRIs emit simultaneously milli- and hundred-Hertz GWs (when the BBHs in them coalesce), we propose the following experiment to test the dispersion relation.

Let us consider two gravitons of difference frequencies, f_e and f'_e . Even if they are emitted at the same time t_e from the same source, they will arrive at the observer with a time delay of

$$\Delta t_a = (1 + Z) \frac{D_0}{2\lambda_g^2} \left(\frac{1}{f_e^2} - \frac{1}{f_e'^2} \right), \quad (7)$$

(Will 1998), where Z is the cosmological redshift, D_0 is a distance scale computed from

$$D_0 = \frac{(1+Z)}{a_0} \int_{t_e}^{t_a} a(t) dt, \quad (8)$$

t_a is the arrival time of the low-frequency wave and $a_0 = a(t_a)$ is the present value of the scale factor. These equations are derived from the simplest model of GW dispersion which has only one parameter λ_g , the Compton wavelength (see Mirshekari et al. 2012, for details). The current limit is $\lambda_g \gtrsim 1.6 \times 10^{13}$ km according to LIGO/Virgo observations (Abbott et al. 2017).

From b-EMRI glitches, we can derive the arrival time of the low-frequency gravitons ($f_e = 10^{-3}$ Hz) to an accuracy of about half a day or less (see Fig. 5). Moreover, using LIGO/Virgo, the arrival time of the high-frequency gravitons ($f'_e = 10^2$ Hz) can be determined to a precision of less than a second. Therefore, we can resolve a minimum Δt_a of about 0.5 day. This resolution corresponds to an upper limit of $1.4 \times 10^{14} (D/100 \text{ Mpc})^{-1/2}$ km for λ_g , where D is the luminosity distance (not to confuse with D_0). This result suggests that if we detect the time delay in the future, we could narrow down the Compton length of gravitons to within one order of magnitude, i.e., $\lambda_g \in (1.6, 14) \times 10^{13} (D/100 \text{ Mpc})^{-1/2}$ km. We note that although the gravitons arrive at different times, they come from the same sky location and luminosity distance. These correlations can be used to corroborate the detection of a real b-EMRI. Alternatively, if no delay is detected, we could as well constrain the Compton wavelength to $\lambda_g > 1.4 \times 10^{14} (D/100 \text{ Mpc})^{-1/2}$ km, which is at least one order of magnitude above the current limit.

Therefore, we conclude that b-EMRIs are interesting new targets for future multi-band observations of GWs. Even with one detection, we can already do three experiments and stringently test our theory of gravitation.

ACKNOWLEDGEMENTS

This work is supported by the NSFC grants No. 11773059, 11273045, 11690023 and 11873022. XC is supported by the ‘‘985 Project’’ of Peking University, and partly by the Strategic Priority Research Program of the Chinese Academy of Sciences through the grants No. XDB23040100 and XDB23010200. WBH is also supported by the Key Research Program of Frontier Sciences of CAS No. QYZDB-SSW-SYS016. The authors thank Xilong Fan for useful discussions.

REFERENCES

Abbott B. P., et al., 2016, *PRX*, **6**, 041015
 Abbott B. P., et al., 2017, *PRL*, **118**, 221101
 Addison E., Laguna P., Larson S., 2015, preprint, ([arXiv:1501.07856](https://arxiv.org/abs/1501.07856))
 Amaro-Seoane P., Chen X., 2016, *MNRAS*, **458**, 3075
 Amaro-Seoane P., Gair J. R., Freitag M., Miller M. C., Mandel I., Cutler C. J., Babak S., 2007, *CQG*, **24**, R113
 Amaro-Seoane P., Brem P., Cuadra J., Armitage P. J., 2012, *ApJ*, **744**, L20
 Babak S., Fang H., Gair J. R., Glampedakis K., Hughes S. A., 2007, *PRD*, **75**, 024005

Babak S., et al., 2017, *PRD*, **95**, 103012
 Baker J. G., Centrella J., Choi D.-I., Koppitz M., van Meter J. R., Miller M. C., 2006, *ApJ*, **653**, L93
 Baker J. G., Boggs W. D., Centrella J., Kelly B. J., McWilliams S. T., Miller M. C., van Meter J. R., 2008, *ApJ*, **682**, L29
 Barack L., Cutler C., 2004, *PRD*, **69**, 082005
 Barausse E., Cardoso V., Pani P., 2014, *PRD*, **89**, 104059
 Blanchet L., Qusailah M. S. S., Will C. M., 2005, *ApJ*, **635**, 508
 Calderón Bustillo J., Clark J. A., Laguna P., Shoemaker D., 2018, *PRL*, **121**, 191102
 Campanelli M., Lousto C. O., Zlochower Y., Merritt D., 2007, *PRL*, **98**, 231102
 Cao Z., Han W.-B., 2017, *PRD*, **96**, 044028
 Centrella J., Baker J. G., Kelly B. J., van Meter J. R., 2010, *RvMP*, **82**, 3069
 Chen X., Han W.-B., 2018, *Comms. Phys.*, **1**, 53
 Chen X., Li S., Cao Z., 2017, preprint, ([arXiv:1703.10543](https://arxiv.org/abs/1703.10543))
 Chua A. J. K., Moore C. J., Gair J. R., 2017, *PRD*, **96**, 044005
 Cutler C., Flanagan É. E., 1994, *PRD*, **49**, 2658
 Damour T., Gopakumar A., 2006, *PRD*, **73**, 124006
 Drasco S., Hughes S. A., 2006, *PRD*, **73**, 024027
 Favata M., Hughes S. A., Holz D. E., 2004, *ApJ*, **607**, L5
 Finn L. S., 1992, *PRD*, **46**, 5236
 Fitchett M. J., 1983, *MNRAS*, **203**, 1049
 Fujita R., Hikida W., Tagoshi H., 2009, *PThPh*, **121**, 843
 Gair J. R., Glampedakis K., 2006, *PRD*, **73**, 064037
 Gair J. R., Vallisneri M., Larson S. L., Baker J. G., 2013, *LRR*, **16**, 7
 Gerosa D., Moore C. J., 2016, *PRL*, **117**, 011101
 Glampedakis K., Kennefick D., 2002, *PRD*, **66**, 044002
 González J. A., Spherhake U., Brüggmann B., Hannam M., Husa S., 2007a, *PRL*, **98**, 091101
 González J. A., Hannam M., Spherhake U., Brüggmann B., Husa S., 2007b, *PRL*, **98**, 231101
 Han W.-B., 2010, *PRD*, **82**, 084013
 Han W.-B., 2014, *IJMPD*, **23**, 1450064
 Han W.-B., Cao Z., 2011, *PRD*, **84**, 044014
 Han W.-B., Cao Z., Hu Y.-M., 2017, *CQG*, **34**, 225010
 Hughes S. A., 2000, *PRD*, **61**, 084004
 Koppitz M., Pollney D., Reisswig C., Rezzolla L., Thornburg J., Diener P., Schnetter E., 2007, *PRL*, **99**, 041102
 Larson S. L., Hiscock W. A., Hellings R. W., 2000, *PRD*, **62**, 062001
 Lousto C. O., Zlochower Y., 2011, *PRL*, **107**, 231102
 Mirshekari S., Yunes N., Will C. M., 2012, *PRD*, **85**, 024041
 Rezzolla L., Barausse E., Dorband E. N., Pollney D., Reisswig C., Seiler J., Husa S., 2008, *PRD*, **78**, 044002
 Schnittman J. D., Buonanno A., 2007, *ApJ*, **662**, L63
 Schnittman J. D., Buonanno A., van Meter J. R., Baker J. G., Boggs W. D., Centrella J., Kelly B. J., McWilliams S. T., 2008, *PRD*, **77**, 044031
 Sesana A., 2016, *PRL*, **116**, 231102
 Sopuerta C. F., Yunes N., Laguna P., 2006, *PRD*, **74**, 124010
 Sundararajan P. A., Khanna G., Hughes S. A., 2007, *PRD*, **76**, 104005
 The LIGO Scientific Collaboration the Virgo Collaboration 2018, arXiv e-prints, ([arXiv:1811.12907](https://arxiv.org/abs/1811.12907))
 Tichy W., Marronetti P., 2008, *PRD*, **78**, 081501
 Wen L., 2003, *ApJ*, **598**, 419
 Will C. M., 1998, *PRD*, **57**, 2061
 van Meter J. R., Miller M. C., Baker J. G., Boggs W. D., Kelly B. J., 2010, *ApJ*, **719**, 1427